1995

AC Impedance Studies on Metal Hydride Electrodes

Wenlin Zhang
Texas A & M University - College Station

M. P. Sridhar Kumar
Texas A & M University - College Station

Supramaniam Srinivasan
Texas A & M University - College Station

Harry J. Ploehn
University of South Carolina - Columbia, ploehn@cec.sc.edu

Publication Info

Journal of the Electrochemical Society, 1995, pages 2935-2943.

Publisher's link: http://dx.doi.org/10.1149/1.2048668
DOI: 10.1149/1.2048668

sushita in its commercial lithium ion product). The latter material has a specific capacity of only about 330 mAh/g. Clearly, we must overcome the high irreversible capacity and the high charging voltages which are present in these carbon-silicon-oxygen glasses before they are commercially relevant. This may be possible once we understand the physics and chemistry of the reversible insertion of lithium in these glassy materials, which is a subject of our ongoing research.

Manuscript submitted March 14, 1995; revised manuscript received April 25, 1995.

Simon Fraser University assisted in meeting the publication costs of this article.

REFERENCES

1. T. Nagaura and K. Tozawa, *Prog. Batt. Solar Cells,* **9,** 209 (1990).
2. I. Kuribayashi, *J. Electron. Eng.,* **30,** 51 (1993).
3. K. Sato, M. Noguchi, A. Demachi, N. Oki, and M.Endo, *Science,* **264,** 556 (1994).
4. S. Yata, H. Kinoshita, M. Komori, N. Ando, T. Kashiwamura, T. Harada, K. Tanaka, and T. Yamabe, *Synth. Met.,* **62,** 153 (1994).
5. Y. Takahashi, J. Oishi, Y. Miki, M. Yoshimura, K. Shibahara, and H. Sakamoto, Paper 2B05, Extended Abstracts, p. 39, 35th Battery Symposium, Japan, Nov. 14-16, 1994.
6. N. Sonobe, M. Ishikawa, and T. Iwasaki, Paper 2B09, p. 47, *ibid.*
7. T. Zheng, Y. Liu, E. W. Fuller, S. Tseng, U. von Sacken, and J. R. Dahn, *This Journal,* **142,** 2581 (1995).
8. R. B. Ellis, U.S. Pat. 2,556,616 (1951).
9. H. Zhang, and C. Pantano, *Mater. Res. Soc. Symp. Proc.,* **271,** 783 (1992).
10. F. I. Hurwitz, J. Z. Gyekenyesi, and P. J. Conroy, *Ceram. Eng. Sci. Proc.,* **10,** 750 (1989); F. I. Hurwitz, L. Hyatt, J. Gorecki, and L. D'Amore, *ibid.,* **8,** 732 (1987).
11. G. T. Burns, R. B. Taylor, Y. Xu, A. Zangvil, and G. A. Zank, *Chem. Mater.,* **4,** 1313 (1992).
12. S. Yajima, J. Hayashi, and M. Omori, *Chem. Lett.,* **9,** 931 (1975).
13. A. M. Wilson, J. N. Reimers, E. W. Fuller, and J. R. Dahn, *Solid State Ionics,* **74,** 249 (1994).
14. H. H. Madden, *J. Vac. Sci. Technol.,* **18,** 667 (1981).
15. L. E. Davis, N. C. MacDonald, P. W. Palmberg, G. E. Riach, and R. E. Weber, *Handbook of Auger Electron Spectroscopy,* 2nd ed., Physical Electronics Div., Perkin Elmer Corp., Eden Prarie, MN (1978).
16. A. M. Wilson and J. R. Dahn, *This Journal,* **142,** 326 (1995).
17. F. Babonneau, G. D. Soraru, G. D'Andrea, S. Dire, and L. Bios, *Mater. Res. Soc. Symp. Proc.,* **27,** 789 (1992).
18. V. Belot, R. J. P. Corriu, D. Leclercq, P. H. Mutin, and A. Vioux, *J. Non-cryst. Solids,* **144,** 287 (1992).
19. F. Babonneau, L. Bios, and J. Livage, *ibid.,* **147/148,** 280 (1992).
20. G. M. Renlund, S. Prochazka, and R. H. Doremus, *J. Mater. Res.,* **6,** 2716 (1991).
21. E. Fitzer, K. Mueller, and W. Schaefer, *The Chemistry of the Pyrolytic Conversion of Organic Compounds to Carbon, in Chemistry and Physics of Carbon Series,* Vol. 7, P. L. Walker, Jr., Editor, p. 237 (1982).
22. B. E. Warren, *Phys. Rev.,* **59,** 693 (1941).
23. P. B. Hirsch, *Proc. Roy. Soc.,* **A226,** 367 (1954).
24. A. F. Wells, *Structural Inorganic Chemistry,* 5th ed., p. 982, Clarendon Press, Oxford (1984).

AC Impedance Studies on Metal Hydride Electrodes

Wenlin Zhang,* M. P. Sridhar Kumar, and Supramaniam Srinivasan****

Center for Electrochemical Systems and Hydrogen Research, Texas Engineering Experiment Station, Texas A&M University System, College Station, Texas 77843-3402, USA

Harry J. Ploehn[a]

Department of Chemical Engineering, Texas A&M University, College Station, Texas 77843, USA

ABSTRACT

The metal hydride (MH_x) electrode is the negative electrode in one of the most advanced secondary batteries (*i.e.,* nickel/metal hydride). The objective of this study is to obtain insight on the mechanism of the hydriding/dehydriding reaction in the battery by using the electrochemical impedance spectroscopy (EIS) technique. An equivalent circuit for the MH_x electrode reaction is proposed. The rate capability of charge and discharge of the MH_x electrode is determined by the kinetics of the charge-transfer reaction at the alloy surface, which is mainly represented by the EIS responses in the low frequency region. Transient and pseudo-steady-state analyses (cyclic voltammetry and potential *vs.* current density behavior) qualitatively and quantitatively support the EIS results. EIS studies on electrodes with (*i*) three types of binding additives, (*ii*) varying amounts of active material, and (*iii*) two types of alloys as active materials demonstrate the usefulness of this technique for developing electrodes with the optimum composition and structure.

Introduction

The nickel metal hydride (Ni/MH_x) battery, developed in recent years, is one of the most promising secondary batteries because of its high energy density, high rate capability, and environmental acceptability.[1-3] The metal hydride electrode is the negative electrode in this battery, with hydrogen being stored in the alloy rather than as compressed gas (as in the nickel/hydrogen batteries). Thus the pressure in the batteries is greatly reduced. A number of rare earth intermetallic compounds with the AB_5 or AB_2 general compositions have been found to absorb and release large amounts of hydrogen rapidly and reversibly.[4,5] It was only as recently as the 1970s [6,7] that these types of alloys were first investigated as hydride electrodes.

The major difference between the hydriding reaction in the electrode and in the gas phase is that the reaction in the former case proceeds via a charge-transfer reaction across the electrode/electrolyte interface, and in the latter case by dissociative adsorption of hydrogen on the alloy surface. The electrode reactions at the negative and positive electrodes in the Ni/MH_x batteries can be expressed by

$$M + H_2O + e^- \leftrightarrow MH + OH^- \quad [1]$$

$$Ni(OH)_2 + OH^- \leftrightarrow NiOOH + H_2O + e^- \quad [2]$$

The mathematical model of Viitanen[8] predicts the polarization behavior of a metal hydride electrode. In this

* Electrochemical Society Student Member.
** Electrochemical Society Active Member.
[a] Present address: Department of Chemical Engineering, University of South Carolina, Columbia, SC 29208, USA.

model, the charge-transfer reaction at the surface of alloys, the diffusion of hydrogen in metal, and the ionic transport in the electrolyte and electronic transport in the solid phase were considered as the intermediate steps of the hydriding/dehydriding reaction. It was concluded that the faradaic process, *i.e.*, the charge-transfer reaction at the surface, is the rate-controlling step. Charge/discharge measurements and cyclic voltammetry have also been previously used to elucidate the mechanisms of the MH_x electrode reaction.[9-11]

Electrochemical impedance spectroscopy (EIS) is an effective technique for analyzing the mechanisms of interfacial electrochemical reactions.[12] Kuriyama *et al.*[13] have used this method for investigating the degradation mechanism of metal hydride electrodes. In their recent work,[14] the activity of the alloy was also analyzed by EIS. The kinetics of the electrochemical hydriding/dehydriding reaction of an alloy electrode was shown to depend on the reaction resistance at the alloy surface. Agarwal *et al.*[15] used a mathematical model to analyze the results of the EIS studies on an $LaNi_5$ ingot-electrode. However, to date, the electrode kinetics of the hydriding/dehydriding reaction have not been well elucidated. Further, it is necessary to draw correlations between the results of EIS studies and the performances of MH_x electrodes.

The purpose of this research is to use the EIS technique to: (*i*) elucidate the mechanism of the hydriding/dehydriding reactions and (*ii*) determine dependence of the kinetics of the reaction on the structure and composition of the MH_x electrodes. Such an analysis is shown to be useful in optimizing the structure and composition of the electrode so as to enhance the performance of the metal hydride electrodes for nickel/metal hydride batteries.

Experimental

The electrochemical cell contained the metal hydride test electrode, a nickel oxide counterelectrode, and a mercury/mercury oxide reference electrode. The metal hydride electrodes were prepared by intimate mixing of the desired amount of the hydrogen storage alloy powder (<45 μm) with a selected additive. The mixture was then pressed at room temperature on both sides of a Ni mesh, producing a sandwich structure with a geometric surface area of 2 cm^2. Before the experiments, the sample electrodes were immersed in the electrolyte for at least 4 h in order to fully wet the electrode. The counterelectrode (sintered NiOOH), obtained from Hughes Aircraft Company, had a much larger geometric area than the working electrode. The electrolyte, 31 weight percent (w/o) of KOH, which is the same as that used in alkaline batteries, was prepared from reagent grade KOH and deionized water. According to the half-cell reactions at the negative and positive electrodes (Eq. 1 and 2), there is no net production or exhaustion of electrolyte species in the cell. Therefore, during the experiments, the electrolyte concentration remained constant.

The experimental setup for the electrochemical measurements consisted of an EG&G Princeton Applied Research M273 potentiostat/galvanostat, M3501A lock-in amplifier, modulated with an IBM PS/2 personal computer with M378 and Headstart software for acquisition of the electrochemical impedance and cyclic voltammetry data. The EIS experiments, under open-circuit conditions, were carried out after a certain number of charge/discharge cycles to ensure that all samples were reproducibly in the highest active and stable states. The impedance data were collected as a function of frequency scanned from the highest (2×10^4 Hz) to the lowest value (1 mHz). The reason for doing this was to avoid any changes in the electrode during the prolonged scanning at very low frequency; however, the probability for such changes is small, as described in following sections. The time for data acquisition in the high frequency domain was less than several minutes; whereas the self-discharge rate of the hydride electrode is at most 2% per day, thus it is reasonable to assume that the electrode condition remains the same after the high frequency test. The variation of the electrode in the total frequency domain with descending frequency scans can thus be expected to be less than with scans in the reverse direction. The amplitude of the sine perturbation signal was 5 mV; this magnitude satisfies the linear polarization requirements. Nyquist plots of the impedance data were then fitted to a proposed equivalent circuit using a nonlinear least square fitting program developed by Macdonald.[16]

Cyclic voltammetry experiments were carried out by scanning the potential at a rate of 1 mV/s between −1.2 and −0.4 V (*vs.* Hg/HgO); this potential range includes that for the operation of MH_x electrodes in the Ni/MH_x batteries and also for other possible reactions during overcharging and overdischarging. Charge/discharge tests of MH_x electrodes were monitored using a Solartron-1286 electrochemical interface at different rates. The cutoff voltage was set at −0.7 V (*vs.* Hg/HgO). Above this value the potential changes rapidly, indicating a complete discharge of the MH_x electrode.

In order to elucidate the mechanism of hydriding/dehydriding reaction, a flat electrode, prepared with the alloy (BNL18: $LaNi_{3.55}Mn_{0.4}Al_{0.3}Co_{0.75}$), was monitored using the EIS technique. For this purpose, an ingot of the metal hydride alloy was mounted in epoxy and then polished with 0.05 μm alumina powder finish. A Ni wire was soldered to this sample for providing electrical contact. In addition to the EIS investigation on the ingot electrode for the elucidation of the mechanism, a similar study was also conducted on the porous metal hydride electrodes. For this purpose, two alloys, with different partial substitution of La and Ni, $La_{0.8}Zr_{0.2}Ni_{3.5}Co_{1.2}Sn_{0.25}$ (BNL17) and $LaNi_{3.55}Mn_{0.4}Al_{0.3}Co_{0.75}$ (BNL18), were used to make porous metal hydride electrodes. The rate capabilities of these electrodes were determined using EIS and cyclic voltammetric techniques. The electrode kinetic parameters were calculated from the results of the EIS and discharge measurements at different rates.

In order to determine the effect of composition and structure on the electrode kinetics using the EIS technique, investigations were made on electrodes: (*i*) containing hydriding alloys with different elemental substitutions; (*ii*) varying the contact area between the current collector and the metal hydride active material; (*iii*) using different binders (Cu powder, high surface area Telflonized carbon Vulcan XC-72R plus 33% of PTFE, or acetylene black) for the active materials; and (*iv*) with different amounts of the active material (Teflonized carbon as binder).

Theoretical Considerations

The hydriding reaction at the electrode/electrolyte interface involves a charge-transfer step followed by a surface to bulk hydrogen atom transfer[17]

$$H_2O + M\ (\text{surface}) + e^- \underset{k_b}{\overset{k_f}{\leftrightarrow}} MH\ (\text{ad., surface}) + OH^- \quad [3]$$

$$MH\ (\text{ad., surface}) + M\ (\text{bulk}) \underset{k'_b}{\overset{k'_f}{\leftrightarrow}} MH\ (\text{ab., bulk}) + M\ (\text{surface}) \quad [4]$$

The charge-transfer step is the same as that for electrolytic hydrogen evolution. The main difference between the hydriding and hydrogen evolution reactions is the second step: in the case of hydriding reaction, the adsorbed hydrogen transfers from the surface to the sites in the host lattice just below the surface, which is then followed by diffusion into the bulk alloy. In the case of the hydrogen evolution reaction, the discharge step is followed by the recombination or electrochemical desorption step to form molecular hydrogen.

In order to analyze and interpret the experimental results, it is necessary to derive a theoretical expression for the impedance for the above processes, which is different from that for a reaction involving only the H_2O charge-transfer step. The degree of coverage, θ, is defined as

$$\theta = \frac{A_{ad.}}{A^0} \quad [5]$$

where A_{ad} and A^0 denote the surface concentration of adsorbed hydrogen and the maximum amount of hydrogen that can be adsorbed on the surface, respectively. The current density for the charge-transfer step can be expressed by the Butler-Volmer equation

$$i = \vec{i} - \overleftarrow{i} = nF\left[k_f C_{H_2O}(1-\theta) \exp\left(-\frac{\alpha nF}{RT}\varphi\right) - k_b C_{OH^-}\theta \exp\left(\frac{\beta nF}{RT}\varphi\right)\right] \quad [6]$$

and for the surface transition reaction by the expression

$$i - k_f'\theta + k_b' C_{MH,bulk}(1-\theta) = nFA^0 \frac{d\theta}{dt} \quad [7]$$

It is reasonable to assume that the diffusion limitations in the electrolyte are negligible because of the high concentrations of H_2O and OH^- at the electrode surface. Thus the current density is a function of the degree of coverage (θ) of adsorbed hydrogen on the surface and the electrode potential (φ). In the ac impedance studies, the variables consist of a steady-state component plus an alternating component

$$i = \bar{i} + \tilde{i} \quad \theta = \bar{\theta} + \tilde{\theta} \quad \varphi = \bar{\varphi} + \tilde{\varphi} \quad [8]$$

Since the time derivative of the steady-state dc component is zero, differentiation of Eq. 6 gives

$$\frac{d\tilde{i}}{dt} = nF\left\{-\left[\frac{\vec{i}}{(1-\theta)nF} + \frac{\overleftarrow{i}}{\theta nF}\right]\frac{d\tilde{\theta}}{dt} - \frac{1}{RT}(\alpha\vec{i} + \beta\overleftarrow{i})\frac{d\tilde{\varphi}}{dt}\right\} \quad [9]$$

$\tilde{i}$, $\tilde{\theta}$, and $\tilde{\varphi}$ change at the same frequencies as expressed by

$$\tilde{B} = B_0 e^{j\omega t} \quad [10]$$

where B represents $\tilde{i}$, $\tilde{\theta}$, and $\tilde{\varphi}$, and B_0 is the amplitude of these variables. The time derivative of Eq. 10 is

$$\frac{d\tilde{B}}{dt} = j\omega\tilde{B} \quad [11]$$

Thus, Eq. 9 can be further simplified as follows

$$\tilde{i} = -\left(\frac{\vec{i}}{(1-\theta)} + \frac{\overleftarrow{i}}{\theta}\right)\tilde{\theta} - \frac{nF}{RT}(\alpha\vec{i} + \beta\overleftarrow{i})\tilde{\varphi} \quad [12]$$

According to the definition of impedance, the interfacial impedance of the MH_x electrode is

$$Z = -\frac{\tilde{\varphi}}{\tilde{i}} \quad [13]$$

From Eq. 12 and 13

$$Z = \frac{RT}{nF(\alpha\vec{i} + \beta\overleftarrow{i})} + \frac{RT}{nF(\alpha\vec{i} + \beta\overleftarrow{i})}\left(\frac{\vec{i}}{(1-\theta)} + \frac{\overleftarrow{i}}{\theta}\right)\frac{\tilde{\theta}}{\tilde{i}} \quad [14]$$

Hence, the contribution to the impedance is due to the faradaic and surface intermediate steps which occur in series. Thus

$$Z = Z_f + Z_{sf} \quad [15]$$

where

$$Z_f = \frac{RT}{nF(\alpha\vec{i} + \beta\overleftarrow{i})} = R_{ct} \quad [16]$$

and

$$Z_{sf} = \frac{RT}{nF(\alpha\vec{i} + \beta\overleftarrow{i})}\left(\frac{\vec{i}}{(1-\theta)} + \frac{\overleftarrow{i}}{\theta}\right)\frac{\tilde{\theta}}{\tilde{i}} \quad [17]$$

where R_{ct} is the charge-transfer resistance, which expresses the kinetics of reaction 3.

In order to obtain the surface impedance, Z_{sf}, the phase transition reaction (Eq. 4) is taken into account. By introducing the alternating component, Eq. 7 can be modified to give

$$(\bar{i} + \tilde{i}) - k_f'(\bar{\theta} + \tilde{\theta}) + k_b' C_{MH,bulk}(1 - \bar{\theta} - \tilde{\theta}) + nFA^0 \frac{d(\bar{\theta} + \tilde{\theta})}{dt} \quad [18]$$

At the equilibrium potential

$$\bar{i} = 0$$

and

$$k_f'\bar{\theta} - k_b' C_{MH,bulk}(1 - \bar{\theta}) = 0 \quad [19]$$

Thus

$$\tilde{i} - k_f'\tilde{\theta} - k_b' C_{MH,bulk}\tilde{\theta} = nFA^0 j\omega\tilde{\theta} \quad [20]$$

and

$$\frac{\tilde{\theta}}{\tilde{i}} = \frac{1}{j\omega(k_f' + k_b' C_{MH,bulk} + nFA^0)} \quad [21]$$

By substituting Eq. 21 into 17, the surface impedance can be expressed as

$$Z_{sf} = \frac{RT}{nF(\alpha\vec{i} + \beta\overleftarrow{i})}\left(\frac{\vec{i}}{(1-\theta)} + \frac{\overleftarrow{i}}{\theta}\right)\frac{1}{j\omega(k_f' + k_b' C_{MH,bulk} + nFA^0)} = \frac{1}{j\omega C_{sf}} \quad [22]$$

where C_{sf} is a pseudo-capacitance of the MH_x electrode due to the surface reaction. At equilibrium

$$i_0 = \vec{i} = \overleftarrow{i} \quad \text{and } \alpha + \beta = 1 \quad [23]$$

and the surface capacitance is

$$C_{sf} = \frac{nF}{RT}\theta(1-\theta)(k_f' + k_b' C_{MH,bulk} + nFA^0) \quad [24]$$

The Randles-Ershler equivalent circuit for the hydriding reaction, proposed in Fig. 1, consists of a charge-transfer resistance, a double-layer capacitance, and a pseudo-capacitance of the surface reaction. It should be pointed out that the diffusion processes in both the electrolyte and the bulk solid are neglected. The rationale for such an assumption is discussed in the next section. The expression for the total impedance of the electrode processes is as follows

$$\frac{1}{Z_t} = \frac{1}{Z_{dl}} + \frac{1}{R_{ct} + Z_{sf}} = \frac{1}{\frac{1}{j\omega C_{dl}}} + \frac{1}{R_{ct} + \frac{1}{j\omega C_{sf}}} \quad [25]$$

where C_{dl} is a double-layer capacitance. Upon rearranging the above equation

$$Z_t = \frac{R_{ct}C_{sf}^2}{(C_{dl} + C_{sf})^2 + (\omega R_{ct}C_{sf}C_{dl})^2} - j\frac{(C_{dl} + C_{sf}) + \omega^2 R_{ct}^2 C_{sf}^2 C_{dl}}{\omega[(C_{dl} + C_{sf})^2 + (\omega R_{ct}C_{sf}C_{dl})^2]} = Z' - jZ'' \quad [26]$$

where

$$Z' = \frac{R_{ct}C_{sf}^2}{(C_{dl} + C_{sf})^2 + (\omega R_{ct}C_{sf}C_{dl})^2} \quad [27]$$

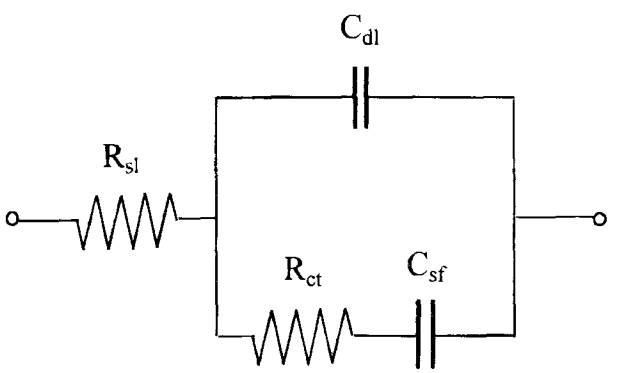

Fig. 1. The Randles-Ershler equivalent circuit model representing the interfacial impedance of an ingot MH_x electrode.

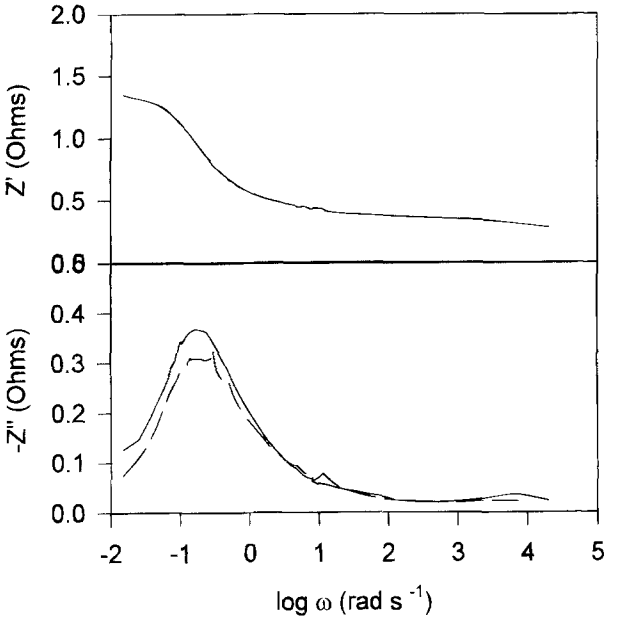

Fig. 2. Kramers-Kronig transforms of impedance data for BNL18 hydride electrode at 50% discharged state. (a, top) Experimental real components of impedance as a function of frequency. (b, bottom) Imaginary components of impedance *vs.* frequency, comparison of experimental data (solid line) with that obtained by KK transformation using real components (dashed line).

and

$$Z'' = \frac{(C_{dl} + C_{sf}) + \omega^2 R_{ct}^2 C_{sf}^2 C_{dl}}{\omega[(C_{dl} + C_{sf})^2 + (\omega R_{ct} C_{sf} C_{dl})^2]} \quad [28]$$

By eliminating the frequency variable (ω), the direct relationship between real and imaginary components of impedance can be expressed by

$$\left(Z' - \frac{R_{ct}C_{sf}}{C_{dl} + C_{sf}}\right)^2 = (Z'')^2\left[\frac{R_{ct}C_{sf}^2}{(C_{dl} + C_{sf})^2} - 1\right] \quad [29]$$

If the pseudo-capacitance of the surface reaction is much larger than the double-layer capacitance, Eq. 29 can be further simplified

$$\left(Z' - \frac{R_{ct}}{2}\right)^2 + (Z'')^2 = \left(\frac{R_{ct}}{2}\right)^2 \quad [30]$$

representing a semicircle in the Nyquist plot from which the charge-transfer resistance can be obtained.

Results and Discussion

The hydride electrode, a stable, linear, and causal system for impedance studies.—The hydrided state of the alloy is generally relatively stable at different states of charge/discharge. This is because the plateau pressures of the investigated hydride alloys are about one atmosphere; thus dehydriding does not occur easily. One supporting evidence for this statement is the self-discharge rate of the alloy sample usually is less than 2% per day. An EIS experiment needs about 1 to 2 h for investigations over the frequency range of 0.001 to 20 kHz. Thus, during this period of time, there is only a slight loss in the capacity of the electrodes. Besides, the impedance data were quite reproducible. For the hydride materials, it usually takes about ten electrochemical charge-discharge cycles for activation of the electrode; after such pretreatment, the electrode shows the highest capacity and the best electrode kinetics. The EIS data were collected after this number of cycles. It is only after prolonged duty cycles that degradation of hydride electrodes occurs. Figure 2 represents the experimental impedance data (solid line) of a metal hydride electrode at 50% state of discharge, for both real and imaginary components, as a function of frequency. The dashed line in (b) is the calculated Z'' *vs.* ω plot, according to Kramers-Kronig transformation, using the real component experimental data. The good agreement between the calculated and experimental data strongly demonstrates that hydride electrodes satisfy the criteria of stability, linearity, and causality for impedance measurements and for the validity of experimental data.[12]

Mechanism of electrode hydriding/dehydriding reaction.—EIS for planar electrode.—The electrochemical impedance spectra were recorded on an ingot of the hydriding alloy (BNL18: $LaNi_{3.55}Mn_{0.4}Al_{0.3}Co_{0.75}$) which simulates a planar electrode. The impedance of the ingot electrode, measured at a potential of −0.7 V *vs.* Hg/HgO reference, is illustrated in the Nyquist plot (Fig. 3). The large semicircle in the low frequency range is consistent with the theoretical model, represented by Eq. 30. Hence, the impedance of the ingot sample is adequately described by the faradaic and surface processes given by Eq. 3 and 4. With the increase of immersion time, the radius of the semicircle decreased in magnitude. This is probably due to an increase in surface roughness near the exposed part of the ingot electrode, because large volume changes occur during charge/discharge cycles. A short 45° linear line (a-b section in Fig. 3) was observed in the Nyquist plot. This behavior cannot be attributed to the Warburg diffusion processes in the electrolyte or in the bulk solid alloy phase. There are two major reasons for this preceding statement: first, the diffusion impedance normally occurs at the lowest frequency for the Randle-Ershler equivalent circuit model; second, a high concentration of the reactant and product species (H_2O and OH^-) are present in the electrolyte. Thus, the impedance due to semi-infinite diffusion of such species in electrolyte is negligible. Further, for the ingot electrode, one may expect a Warburg impedance due to the diffusion of H atoms into the bulk alloy which is a one-dimensional semi-infinite or finite diffusion. According to Fig. 3, no specific Warburg impedance in the low frequency range was observed, probably because the diffusion rate of hydrogen into the bulk alloy is relatively fast. Thus, the equivalent circuit model, shown in Fig. 1, which characterizes the charge-transfer and surface processes, is appropriate for the analysis of the impedance results. The reason for the small impedance in the highest frequency range (a-b section) is not clear at the present time.

EIS on porous electrodes.—EIS were also recorded on porous electrodes prepared according to the description in the Experimental section. A typical Nyquist plot for a porous metal hydride electrode shows two small arcs in the high frequency region and one large arc in the low frequency region (Fig. 4a). Thus, there are at least three dis-

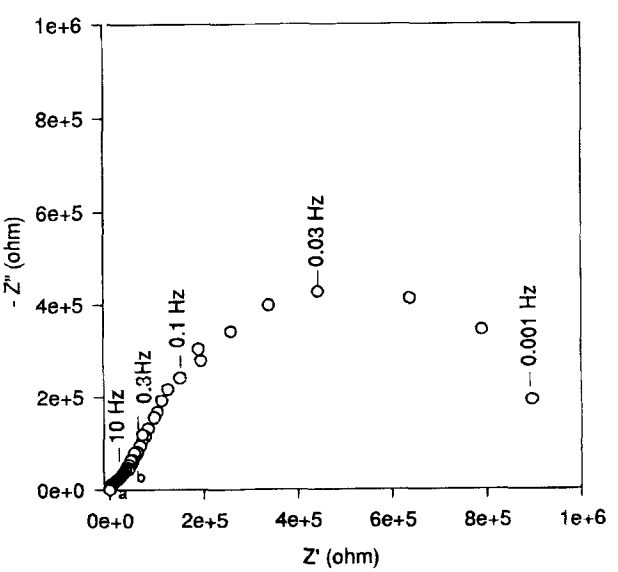

Fig. 3. Nyquist plot for ingot sample (BNL18: $LaNi_{3.55}Mn_{0.4}Al_{0.3}Co_{0.75}$) with surface area of 2 mm² at −0.7 *vs.* Hg/HgO reference electrode.

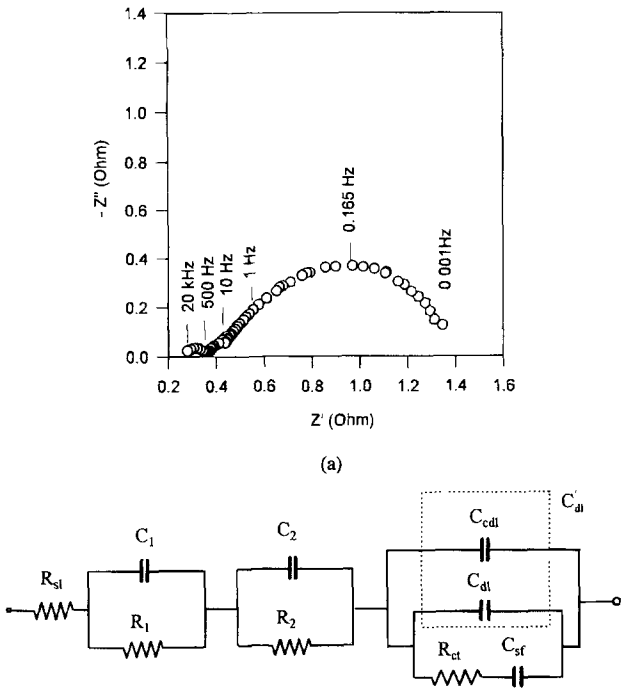

Fig. 4. (a) Typical Nyquist plot of MH_x electrode with three distinguished time constants and (b) the proposed equivalent circuit.

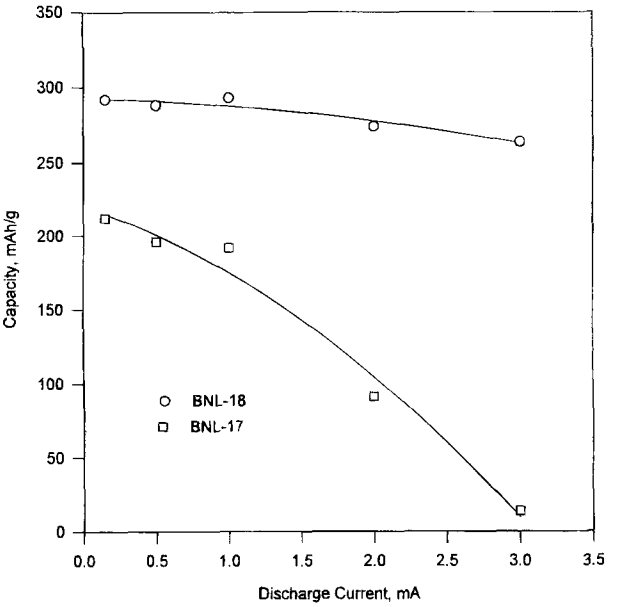

Fig. 5. Rate capabilities of hydride electrodes with two alloys.

tinct relaxation processes. The largest arc exhibits an initially short linear region with a slope of about 45°. Kuriyama *et al.*[13] found a similar impedance response. These workers attributed the 45° linear line to Warburg diffusion without taking into account the porous structure of the MH_x electrode. According to de Levie,[17] a 45° line is also a characteristic impedance response of an electrode with a cylindrical pore structure. Comparing the Nyquist plots for the planar electrode (Fig. 3), where no specific Warburg diffusion impedance was observed, and for the porous electrode (Fig. 4a), it may be concluded that the linear region in the Nyquist plot in the latter case is primarily due to the porous structure of the electrode. The impedance in the low frequency region represents the charge-transfer step at the electrode/solution interface and the surface transition reaction; there is no rate limitation due to the diffusion of species in the electrolyte or the diffusion of hydrogen into the alloy particle.

Two alloy samples were selected to further investigate the electrode kinetics of the hydriding/dehydriding reactions: BNL17 (La-Zr-Ni-Co-Sn) and BNL18 (La-Ni-Co-Mn-Al). Figure 5 shows the results of experiments conducted on electrodes with the BNL17 and BNL18, as active materials, to determine the effect of discharge rate on the capacity. For the electrode with BNL18, over 90% of capacity could be obtained even at the 3 C rate of discharge. However, with BNL17, the capacity decreases considerably at higher discharge rates. At the 3 C rate, its capacity was almost zero.

The rate capabilities of these electrodes depend on the kinetics of the hydriding/dehydriding reactions. EIS tests were thus performed on these electrodes under open-circuit conditions at different depths of discharge. The high frequency relaxation processes, corresponding to the contact impedance (discussed later) did not change with the depth of discharge. As mentioned previously, the semicircles at low frequencies are attributed to the relaxation of faradaic and surface processes. The Nyquist plots show considerably larger semicircles for the BNL17 than for the BNL18 electrode at all depths of discharge. Figure 6 represents the Nyquist plots at about 50% depth of discharge for both electrodes. An equivalent circuit model, as shown in Fig. 4b, was used to obtain the electrode kinetic parameters. The contact impedance between the current collector and the sample (alloy + binder) corresponds to R_1 and C_1 in the model. R_2 and C_2 represent the contact impedance between alloy particles in the electrode. The charge-transfer resistance, double-layer capacitance, and the surface capacitance are designated by R_{ct}, C_{dl}, and C_{sf}, respectively, for the proposed Randles-Ersher equivalent circuit (Fig. 1). Since the carbon additive (Vulcan-XC-72R) is also in contact with the electrolyte but does not undergo a faradaic reaction, only the double-layer capacitance of carbon, C_{cdl}, need be considered: this capacitance, along with the double-layer capacitance of the alloy, is in parallel. The double-layer capacitance of carbon matrix, C_{cdl}, and that for the active alloy, C_{dl}, were treated as a single capacitance C'_{dl}

$$C'_{dl} = C_{dl} + C_{cdl} \quad [31]$$

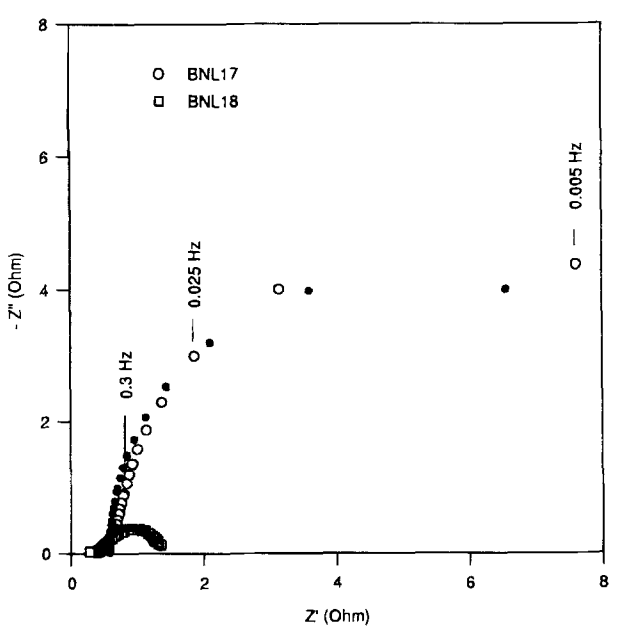

Fig. 6. Nyquist plots demonstrating slow and fast kinetics of charge-transfer step of hydride electrodes with two alloys (BNL17 and BNL18, state of charge of electrode: 50%). Solid points are the fitting results.

Table I. Charge-transfer resistance obtained by EIS and pseudo-steady-state methods, electrode, 75 mg of active alloy (BNL17, 18) and 75 mg binder material (Teflonized Vulcan XC-72R).[a]

Sample	R_{sl} (Ω)	R_{ct} (Ω)	C'_{dl} (F)	C_{sf} (F)	R_{ct} (Ω)
	(from EIS)				(from Tafel Plot)
BNL17	0.5812	8.1981	1.5987	16.572	10.7 ± 2.0
BNL18	0.4742	0.7931	1.7804	12.995	1.08 ± 0.2

[a] The contact impedances which hardly changed with different alloys are not listed.

The resistance, R_{Sl}, measured at the highest frequency, is the electrolyte resistance between the working and reference electrodes.

A nonlinear least square data fitting routine, using the above equivalent circuit, gave a good fit to the experimental Nyquist plots. The fitting of the larger semicircle was carried out by treating the porous structure of MH_x electrode, to a first approximation, as a flat electrode with a large surface area, because the most significant response occurs in the low frequency range where the high penetration depth condition is satisfied.[17] The fitted values of the parameters in the equivalent circuit are listed in Table I. The charge-transfer resistances are larger for BNL17 than for BNL18 electrode at all depths of discharge (Fig. 7). These results are consistent with those of the rate capability measurements. Further, the reaction resistance in the fully discharged state (capacity equals zero) increases to a very high value, probably because of some passive film of oxide forming on the surface. Assuming that the specific double-layer capacitance of the active alloy is in the range of the generally accepted value of 20 μF/cm^2 for a planar metal surface, the calculated value for 75 mg of alloy having an average particle radius of 5 μm is about 0.001 F. This value is much smaller than the obtained value of C'_{dl}. Hence, the main contribution to C'_{dl} is from the carbon matrix (Eq. 31). On the other hand, the pseudo-capacitance of the surface reaction, C_{sf}, is much higher than the double-layer capacitance, which is consistent with the assumption in the theoretical section. From Table I, it can be seen that except for the charge-transfer resistance, R_{ct}, there is hardly any change in any of the other equivalent circuit parameters. The parameter R_{ct} reflects the electrocatalytic activity of the hydride alloy, while all other parameters are probably related to the structure of porous electrode.

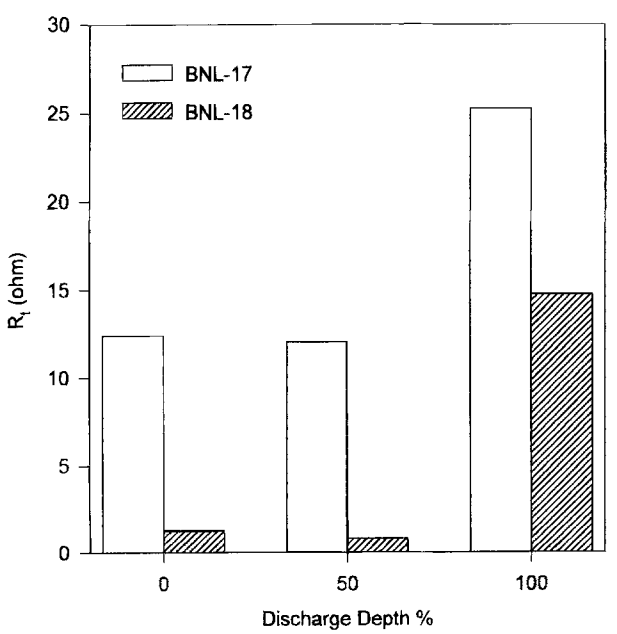

Fig. 7. Charge-transfer resistance of hydride electrodes with BNL17 and BNL18 alloys at different depths of discharge.

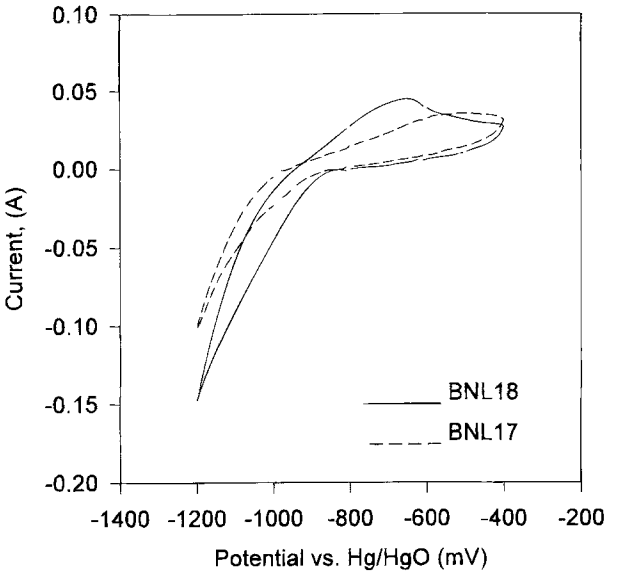

Fig. 8. Cyclic voltammograms during hydriding/dehydriding for hydride electrodes, potential sweep rate = 1 mV/s.

Justification of interpretation of mechanisms from impedance data.—Analysis of EIS data could lead to multiple interpretations of mechanism of reactions. However, if we analyze the data logically, change the experimental conditions or use other techniques, it is possible to minimize the uncertainty. The logic of our analysis was to propose an impedance model, based on the results of other researchers,[8,9-11,14,17] which are well accepted in the case of the hydrogen evolution reactions. For the hydriding reaction, the first step is the same as for hydrogen evolution, *i.e.*, charge-transfer. However, for the hydriding reaction, hydrogen adsorption and absorption are the subsequent steps. There could, however, be several possibilities to fit one set of data. Thus, the final and the most important analysis was to verify the model using other experimental techniques and under other conditions. In this work, five methods were applied to evaluate the equivalent circuit model.

1. The planar electrode, investigated because of its simple structure, was compared to the porous electrode. For the planar electrode, the specific Warburg diffusion impedance was not detected (Fig. 3) and thus the equivalent circuit corresponds to one without diffusion control.

2. The impedances were measured at different states of discharge (Fig. 7) first to compare the impedance change of selected samples and then to elucidate the reaction mechanisms.

3. Cyclic voltammetry studies also showed that for the hydriding reaction, the BNL18 electrode is a better electrocatalyst than the BNL17 electrode (Fig. 8). During scanning in the negative direction, the current increased rapidly when the potential decreased below about −0.9 V (*vs.* Hg/HgO). This current increase is due to the contribution of hydrogen evolution reaction. During the reverse scan, a broad peak was observed for the dehydriding reaction. The position of this peak reflects the overpotential for this reaction and qualitatively provides the information on the kinetics of the electrode reaction.[18] The peak for the BNL18 electrode is at a more negative potential than that for the BNL17 electrode, again showing a higher charge-transfer rate in the former case.

4. The plots of the pseudo-steady state potential *vs.* discharge current, *i.e.*, Tafel plots, for these electrodes are shown in Fig. 9. The exchange current for the dehydriding reaction is an order of magnitude higher on the BNL18 than on the BNL17 electrode. From Eq. 16 and at a potential close to the reversible potential, the relationship between charge-transfer resistance and exchange current density can be expressed by

$$R_{ct} = \frac{RT}{nFi_0} \quad [32]$$

The charge-transfer resistances calculated from the exchange current densities are quite consistent with those obtained from fitting of the EIS data (Table I).

5. Finally, the theory was applied to the metal hydride electrodes to determine the effect of structure and composition on the performance of electrodes. (Please see next subsection.)

In a separate investigation,[19] the effect of temperature on the performance of hydride electrodes was determined. It was found that the higher the temperature, the smaller is the charge-transfer resistance represented by the semicircle in the low frequency range. The activation energy, calculated using the Arrhenius equation, is too high for diffusion control. In our previous work,[20] the effects of Sn, Ce, Co substitution on the rate capability were reported. The correlation between the rate capability and the charge-transfer resistance, determined using the EIS technique, was very good. All of these support our conclusion that the charge-transfer step is rate determining. Because of the consideration of length of our paper, such results were not included in this paper.

Structure and composition of metal hydride electrode.—EIS measurements were carried out to investigate the effect of the structure and composition of the metal hydride electrode on the kinetics of the hydriding/dehydriding reaction. These tests also provide useful information for better design of electrodes.

Contact impedance between Ni mesh (current collector) and electrode materials.—The active material and Vulcan + 33% PTFE (a binding material) were pressed onto Ni mesh substrates of two different sizes. The Nyquist plots are illustrated in Fig. 10. For the sample with larger contact area with Ni mesh (2 cm^2), the diameter of the semicircle in the higher frequency range (>520 Hz), is smaller than that for the sample with a contact area of 0.5 cm^2 (frequency > 126 Hz). The loop in the higher frequency range probably represents an impedance between the current collector and the active material, *i.e.*, the impedance of the substrate as defined by Lenhart and Macdonald.[21] This contact impedance is inversely proportional to the total contact area of the active material with the current collector. The diameter of the arc in the intermediate frequency range (>20 Hz) does not depend on the contact area (Fig. 10).

Effect of binder materials.—Electrodes were made using Cu powder, Vulcan (XC-72R) or acetylene black as the binder material. EIS results on these electrodes are presented in Fig. 11. The plots show that the impedance in the intermediate frequency range (11.3 to 126 Hz) decreases in the following order

acetylene black > Vulcan (XC-72R) > Cu powder

This order is in accordance with the increasing electronic conductivity of the binder material. Cu is a very good electronic conductor, and the conductivity of Vulcan (XC-72R) is higher than that of acetylene black. The semicircle in the middle frequency range appears to be related to the electronic conductivity of MH_x electrodes. In a previous study, Kuriyama *et al.*[13] assigned the two smaller arcs in the higher frequency region to contact impedance; this interpretation is confirmed by our experimental results. In the highest frequency region, the impedance for Cu powder is very small (Fig. 11), because the high electronic conductivity of Cu powder provides the best contact between the current collector and the active material. This again supports the view that the contact impedance is represented by the arc in the high frequency region.

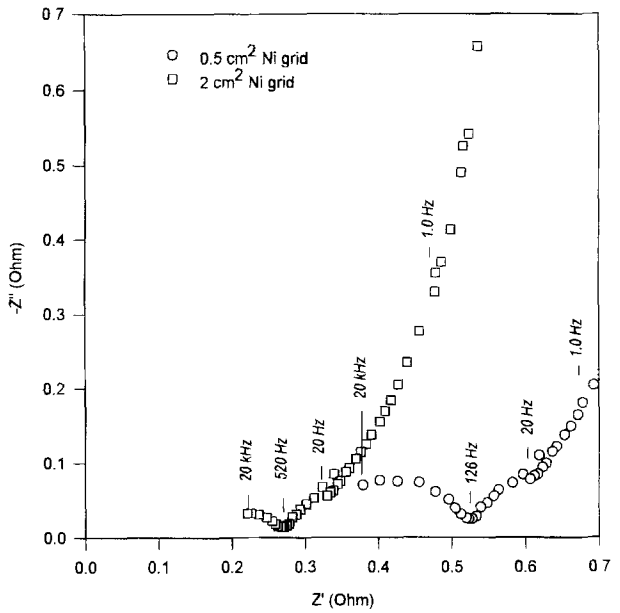

Fig. 10. Effect of area of Ni grid current collector on EIS. Hydride electrodes with same amount of alloy (BNL18) and binder material.

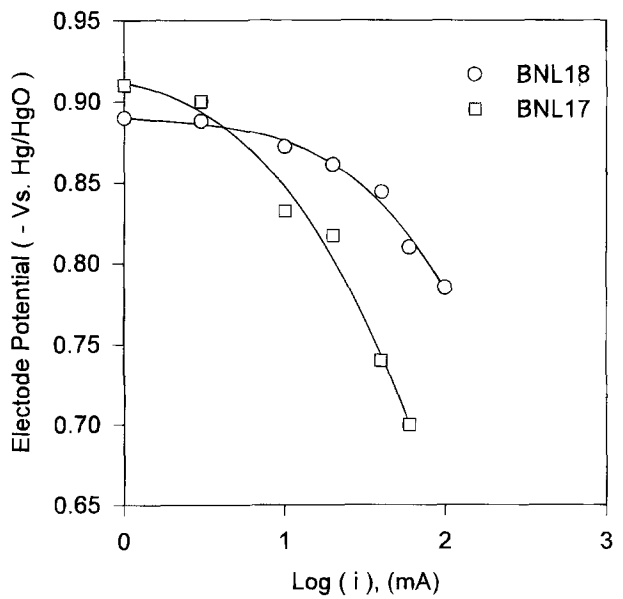

Fig. 9. Electrode potential *vs.* current density plots during discharge of hydride electrodes containing two alloys (BNL17 and BNL18).

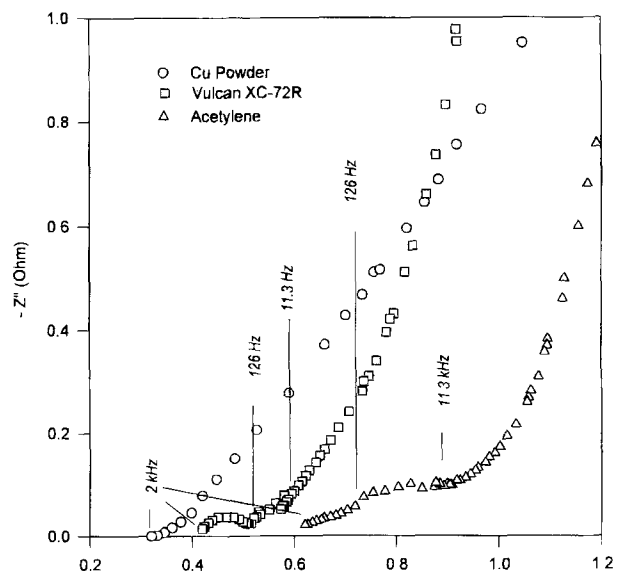

Fig. 11. Effect of binder materials on EIS for hydride electrodes.

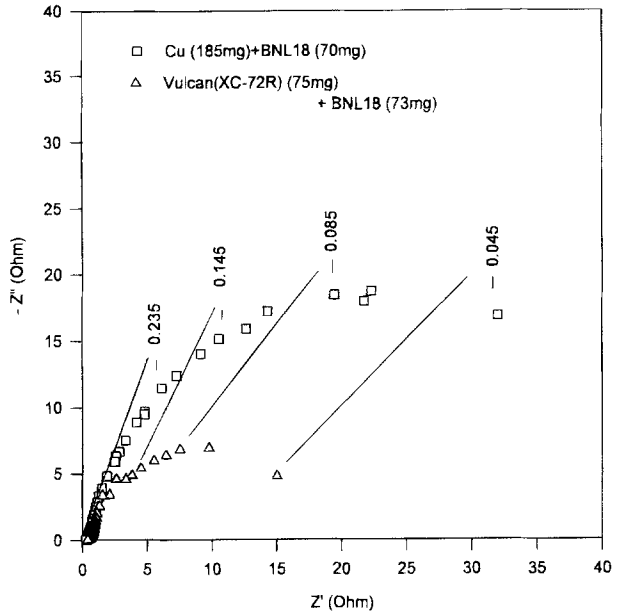

Fig. 12. Nyquist plots (low frequency region) for hydride electrodes with Cu and Vulcan (XC-72R) as the binder material. The data in the graph represent the frequency (Hz).

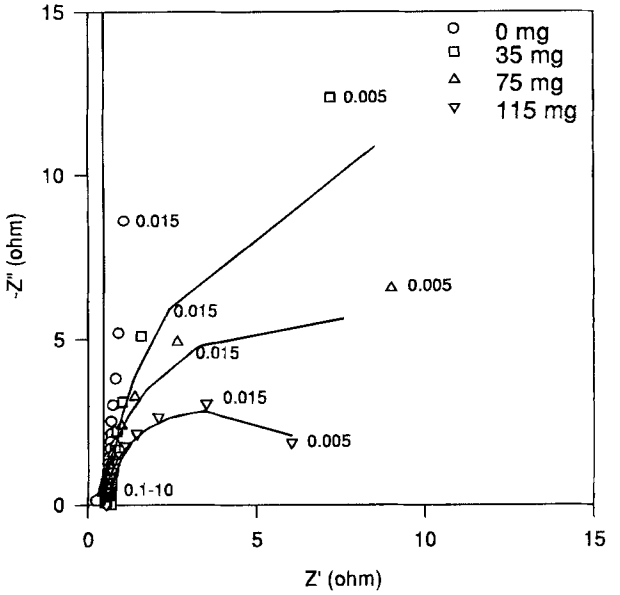

Fig. 13. Effect of amount of active material (BNL26: La-Ni-Sn) in hydride electrode on EIS. The data in the graph represent the frequencies (Hz). The solid lines demonstrate the theoretical predictions.

From the above discussion, it appears that Cu should be a good binder for the MH_x electrode. However, previous work,[21] conducted in our laboratory, demonstrated that the Teflonized Vulcan (XC-72R) is a better candidate, as evidenced by the superior discharge performance of an electrode with this additive. This discrepancy can be explained by the EIS results in the low frequency region (<11.3 Hz) (Fig. 12). At low frequencies, the impedance of the electrode with Cu powder has a larger value than with the Teflonized Vulcan (XC-72R) binder. As stated in the previous subsection, the semicircle in the low frequency region is assumed to represent the faradaic process at the electrode/electrolyte interface. Since the same amount of the identical material (BNL18) was used in both cases, this result can be rationalized on the basis of a higher electrochemically active surface area of the electrode with the Teflonized Vulcan (XC-72R). Teflonized Vulcan (XC-72R) has a much higher porosity and surface area than Cu powder, and thus the electrode with the former binder can be expected to have a higher electrochemically active surface area than the latter.

Effect of amount of alloy.—In order to determine the best structure of the metal hydride electrode, electrodes made by mixing different amounts of alloys with Vulcan XC-72R (75 mg) were tested. The Nyquist plots for these electrodes, containing 0, 35, 75, and 115 mg of the powder alloy, respectively, are shown in Fig. 13. The most significant changes of the equivalent circuit elements, with the variation of the amount of alloy, are in the low frequency region (<10 Hz). Table II shows the dependence of the values of the equivalent circuit parameters on the amount of alloy in the electrode. The double-layer capacitance, C'_{dl}, hardly changes with the amount of alloy since its main contribution is from the high surface carbon matrix (Vulcan XC-72R). For the electrode without active material, the impedance behavior is that of a pure double-layer capacitance, *i.e.*, an infinite charge-transfer resistance (Fig. 13). With an increasing amount of the alloy, the diameter of the semicircle decreases. A larger amount of alloy provides more active sites; assuming the reaction rate per unit particle area to be constant, the total charge-transfer resistance should decrease proportionally with an increasing amount of the alloy.

In contrast, the pseudo capacitance of the surface process should increase proportionally with the active surface area of alloy particles. The charge-transfer resistance and the pseudo capacitance of the surface process as a function of the amount of alloys, obtained from the data-fitting program, are shown in Fig. 14. As expected, there was a considerable decrease in the charge-transfer resistance and an increase in the pseudo capacitance of the surface process with an increasing amount of alloy. However, the charge-transfer resistance and the pseudo capacitance of the surface process increased more gradually when the amount of alloy was increased above 75 mg. This observation strongly suggests that the porosity of electrode and the specific exposure area of alloy to the electrolyte do not increase further above this amount. The impedance results confirm the results of our previous investigation on the optimization of composition of the hydride electrode,[20] where it was shown that the specific capacity had a maximum value at about 75 mg of the alloy/cm^2 of electrode.

Conclusions

EIS experiments were conducted on metal hydride electrodes to elucidate the mechanism of hydriding/dehydriding reactions and to determine the usefulness of this technique to optimize the composition and structure of these electrodes. The important conclusions from these studies can be summarized as follows.

The impedance of metal hydride electrodes is mainly determined by the faradaic process in the low frequency region. The exchange current, obtained using EIS and pseudo-steady-state techniques, are in agreement. The charge-transfer resistance is practically independent of the state of discharge.

There is also a good correlation between the rate capability and the charge-transfer reaction rate at the alloy surface.

Table II. The parameters obtained by EIS on metal hydride electrode containing different amount of active alloy and 75 mg binder material (Teflonized Vulcan XC-72R).[a]

Amount of alloy	R_{sl} (Ω)	R_{ct} (Ω)	C'_{dl} (F)	C_{sf} (F)
Pure C	0.4395	—	1.4093	—
35 mg	0.6534	21.674	1.5986	6.2189
75 mg	0.4759	11.011	1.5714	12.881
115 mg	0.4871	6.516	1.4511	14.21

[a] The contact impedances, which hardly changed with different amounts of alloys are not listed.

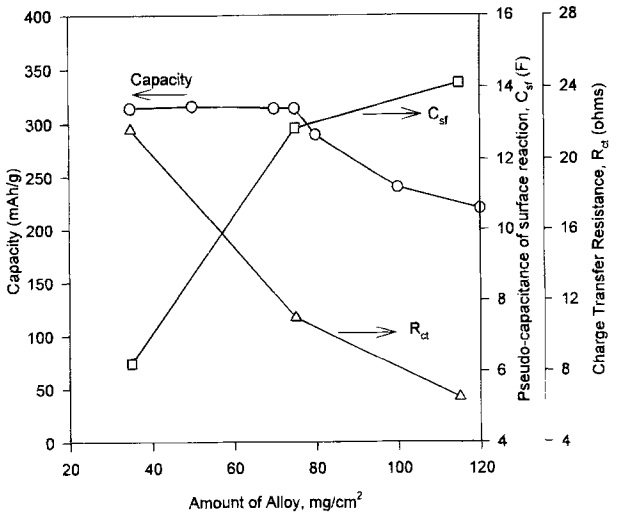

Fig. 14. Correlations of EIS parameters with capacities of hydride electrode containing BNL26 (La-Ni-Sn),

The EIS technique also confirmed our previous results that Vulcan (XC-72R) is a better binder material than copper powder or acetylene black.

Charge/discharge tests showed that an optimum amount of alloy for a unit geometric area of the electrode yields the highest performance. An analysis of the EIS results shows that the electrode with this optimum amount has the highest pseudo capacitance for the surface reaction per gram of alloy and the lowest specific charge-transfer resistance; these results thus support the conclusions reached in our previous charge/discharge studies.

Acknowledgments

The authors wish to acknowledge the sponsorship of this work by the Chemical Sciences Division, Office of Basic Energy Sciences, U.S. Department of Energy (Contract No. DE-FG03-93ER14381). The work carried out by one of us (W. Z.) was in partial fulfillment of the requirements for the Ph.D. degree in Chemical Engineering. The authors are also grateful to Dr. Darrel F. Untereker and a reviewer for their constructive criticisms and suggestions, which led to the subsections: "The Hydride Electrode, a stable linear and causal system for impedance studies" and "Justification of interpretation of mechanisms from impedance data."

Manuscript submitted Oct. 6 1994; revised manuscript received April 24, 1995. This was Paper 593 presented at the San Francisco, CA, Meeting of the Society, May 17-22, 1994.

Texas A&M University assisted in meeting the publication costs of this article.

LIST OF SYMBOLS

A_{sf}	surface concentration of adsorbed H
A^0	maximum surface concentration of adsorbed H
C_{cdl}	double-layer capacitance of carbon matrix
C_{dl}	double-layer capacitance of alloy
C'_{dl}	total double-layer capacitance
C_{H_2O}	concentration of H_2O in electrolyte
$C_{MH,bulk}$	concentration of H in bulk MH alloy
F	Faraday constant
i	current density, A/cm^2
i_0	exchange current density, A/cm^2
j	$\sqrt{-1}$
k_b	backward rate constant in Eq. 3
k'_f	forward rate constant in Eq. 4
k'_b	backward rate constant in Eq. 4
k_f	forward rate constant in Eq. 3
n	number of electron transferred
R	gas constant
R_{ct}	charge-transfer resistance
T	temperature
Z	impedance
Z'	real component of impedance
Z''	image component of impedance
Z_f	faradaic impedance
Z_{sf}	impedance of surface processes
Z_t	total impedance of MH electrode

Greek

α	charge-transfer coefficient in reduction direction
β	charge-transfer coefficient in oxidation direction
θ	coverage degree of adsorbed hydrogen
φ	electrode potential
ω	angular frequency of ac single

Superscripts

$\rightarrow$	reduction direction
$\leftarrow$	oxidation direction
$-$	dc single
$\sim$	ac single

REFERENCES

1. J. G. Willems and K. H. Buschow, *J. Less-Common Met.*, **129,** 13 (1987).
2. M. A. Fetcenco, S. Venkatesan, K. C. Hong, and B. Reichman, in *Proceedings of the 16th International Power Sources Symposium,* p. 441 (1988).
3. A. Anani, A. Visintin, S. Srinivasan, A. J. Appleby, and H. S. Lim, *This Journal,* **139,** 985 (1992).
4. J. H. N. Van Vucht, F. A. Kuijpers, and H. C. A. M. Bruning, *Philips Res. Rep.,* **25,** 133 (1970).
5. *Proceedings of International Symposium on Hydrides for Energy Storage,* H. H. van Mal, A. R. Miedema, A. F. Andresen, and A. J. Maeland, Editors, p. 251, Pergamon Press, Ltd., Oxford (1978).
6. H. H. Ewe, E. W. Justi, and K. Stephan, *Energy Conver.,* **13,** 109 (1973).
7. E. W. Justi, H. H. Ewe, A. W. Kalberlah, N. M. Saridakis, and M. H. Schaefer, *ibid.,* **10,** 183 (1970).
8. M. Viitanen, *This Journal,* **143,** 936 (1993).
9. H. Ogawa, M. Ikoma, H. Kawano, and I. Matsumoto, in *Proceedings of the 16th International Power Sources Symposium,* p. 393 (1988).
10. T. Sakai, H. Ishikawa, H. Miyamura, and N. Kuriyama, *This Journal,* **138,** 908 (1991).
11. T. Ikeya, K. Kumai, and T. Iwahori, *ibid.,* **140,** 3082 (1993).
12. *Impedance Spectroscopy,* J. R. Macdonald, Editor, John Wiley & Sons, Inc., New York (1986).
13. N. Kuriyama, T. Sakai, H. Miyamura, I. Uehara, H. Ishikawa, and T. Iwasaki, *This Journal,* **139,** L72 (1992).
14. N. Kuriyama, T. Sakai, H. Miyamura, I. Uehara, H. Ishikawa, and T. Iwasaki, *J. Alloys Comp.,* **192,** 161 (1993).
15. P. Agarwal, M. E. Orazem, and A. Hiser, in *Hydrogen Storage Materials, Batteries, and Electrochemistry,* D. A. Corrigan and S. Srinivasan, Editors, PV 92-5, p. 120, The Electrochemical Society Proceedings Series, Pennington, NJ (1992).
16. R. Macdonald, *J. Electroanal. Chem.,* **131,** 77 (1982).
17. R. de Levie, in *Advances in Electrochemistry and Electrochemical Engineering,* Vol. 6, P. Delahay, Editor, Chap. 4, John Wiley & Sons, Inc., New York (1967).
18. *Electrochemical Methods,* A. J. Bard and L. R. Faulkner, Editors, John Wiley & Sons, Inc., New York (1980).
19. M. P. S. Kumar, W. Zhang, and S. Srinivasan, Abstract 4, p. 6, The Electrochemical Society Extended Abstracts, Vol. 95-1, Reno, NV, May 21-26, 1995.
20. M. P. S. Kumar, W. Zhang, K. Petrov, A. A. Rostami, and S. Srinivasan, *This Journal,* In press.
21. S. J. Lenhart, D. D. Macdonald, and B. G. Pound, *This Journal,* **135,** 1063 (1988).
22. K. Petrov, A. Visintin, S. Srinivasan, and A. J. Appleby, Abstract 27, p. 41, The Electrochemical Society Extended Abstracts, Vol. 93-1, Honolulu, HI, May 16-21, 1993.